01 Jan 2022

The Effects Of Mixing Multi-component HLW Glasses On Spinel Crystal Size

C. (Charmayne) E. Lonergan
Missouri University of Science and Technology, clonergan@mst.edu

J. Rice

C. Skidmore

M. J. Schweiger

et. al. For a complete list of authors, see https://scholarsmine.mst.edu/matsci_eng_facwork/3218

Recommended Citation

C. E. Lonergan et al., "The Effects Of Mixing Multi-component HLW Glasses On Spinel Crystal Size," *Journal of Nuclear Materials*, vol. 558, article no. 153318, Elsevier, Jan 2022.
The definitive version is available at https://doi.org/10.1016/j.jnucmat.2021.153318

Journal of Nuclear Materials 558 (2022) 153318

Contents lists available at ScienceDirect

Journal of Nuclear Materials

journal homepage: www.elsevier.com/locate/jnucmat

The effects of mixing multi-component HLW glasses on spinel crystal size

C.E. Lonergan*, J. Rice, C. Skidmore, M.J. Schweiger, P. Hrma

Pacific Northwest National Laboratory, 902 Battelle Blvd, Richland, WA 99354, United States

ARTICLE INFO

Article history:
Received 15 April 2021
Revised 24 August 2021
Accepted 25 September 2021
Available online 27 September 2021

Keywords:
Spinel size
HLW glasses
Spinel
Crystal size

ABSTRACT

The Hanford Waste Treatment and Immobilization Plant will vitrify radioactive waste into borosilicate glass. The high-level waste (HLW) glass formulations are constrained by processing and property requirements, including restrictions aimed at avoiding detrimental impacts of spinel crystallization in the melter. To understand the impact of glass chemistry on crystallization, two HLW glasses precipitating small (~5 μm) spinel crystals were individually mixed and melted with a glass that precipitated large (~45 μm) spinel crystals in ratios of 25, 50, and 75 wt%. The size of spinel crystals in the mixed glasses varied from 5 to 20 μm. Small crystal size was attributed to: (1) high concentrations of nuclei due to the presence of ruthenium oxide and (2) chromium oxide aiding high rates of nucleation. Results from this study indicate that the spinel crystal size can be controlled using chromium oxide and/or noble metal concentrations in the melt, even in complex mixtures like HLW glasses. Smaller crystals tend to settle more slowly than larger crystals, therefore smaller crystals would be more acceptable in the melter without a risk of failure. Allowing higher concentrations of spinel-forming waste components in the waste glass enables glass compositions with higher waste loading, thus increasing plant operational flexibility. An additional benefit to the presence of chromium oxide in the glass composition is the potential for the oxide to protect melter walls against corrosion.

1. Introduction

On the Hanford Site in Richland, WA, approximately 56 million gallons of radioactive wastes are stored in 177 tanks [1]. Portions of this waste will be vitrified into high-level waste (HLW) glasses [2,3]. The glass waste forms will be formulated to meet regulatory limits, to be processable in a joule-heated melter, and to obtain high waste loading [4–7]. Spinel crystallization during melting and idling of the melter is a HLW glass processing concern because spinel settling may cause shorting of the electrodes and block the discharge port of the melter [4,5,8–11].

Previously suggested mitigation strategies, such as limiting crystal fraction to less than 1 vol% at 950 °C [12], or limiting liquidus temperature (T_L) to less than 1050 °C, are conservative. The above protocols impose excessive restriction on waste loading, leading to the production of substantially greater numbers of glass canisters, higher operation costs, and an increase in the Hanford mission lifetime [13]. Constraints involving spinel settling behavior would likely be less restrictive and more able to address the potential risk to melter operations.

The rate of undisturbed settling for multiple crystals is given by Stokes' law in the form:

$$r = \frac{k_h k_s g(\rho_s - \rho_l)a^2}{\eta} \quad (1)$$

where r is the settling rate (m/s), k_h is the hindrance factor (unitless), k_s is the particle shape factor (unitless), g is the gravity acceleration (m/s^2), ρ_s is the solid density (kg/m^3), ρ_l is the liquid density (kg/m^3), α is the particle diameter (m), and η, is the melt viscosity (Pa•s). Further description of this relationship can be found in the literature [14]. As Stokes' law suggests, settling rate is proportional to the square of the crystal size. Thus, decreasing the crystal size ten times reduces the settling rate by a factor of 100. At this rate, crystals will not settle on the melter bottom or in the melt discharge port, but will be removed with the melt when poured into the canisters.

For any melt composition, the equilibrium crystal size depends on the number density of crystal nucleation sites and the con-

* Corresponding author.
E-mail address: charmayne.lonergan@pnnl.gov (C.E. Lonergan).

https://doi.org/10.1016/j.jnucmat.2021.153318
0022-3115/

tent of crystal-forming components in the melt [15]. Therefore, the amount of crystalline phase is a function of the difference between the heat treatment temperature and the T_L. Consequently, the heat treatment temperature has a strong impact on the crystal size. For a variety of glass compositions, Riley et al. [16] observed ~5 μm crystals forming at 1000 to 1200 °C and ~30 μm crystals forming at temperatures above 1300 °C. These results confirm that crystal size is determined by the rate of nucleation, which increases as the heat-treatment temperature decreases, even though the total mass of crystals was smaller at higher temperatures.

Apart from the temperature history of cooling, the main factor influencing the size and amount of spinel phase formation is the melt composition. Alton et al. [15] studied the effect of various components on spinel crystal size, concluding, that nucleation agents such as platinum group metals (Ru, Rh, Pt) and Cr, provide nucleation sites that allow crystals to start growing in large numbers as soon as the temperature drops below the liquidus. The large crystal number density strongly limits the final crystal size from the crystal-forming material available in the melt.

A previous study [17] showed that ~5 μm sized spinel crystals precipitated in HLW glasses over an extended glass composition region. These results conflicted with earlier studies [18–20] reporting spinel crystals sizes up to ~100 μm. Matyas et al. [20] showed for the HLW glass Ni1.5, which contains high nickel oxide concentrations (1.5 wt%) that the average size of spinel crystals was 92 μm ±18–20 μm depending on heat treatment time and the selected dopants. In the same study [20], increasing the concentration of Cr_2O_3 (from 0.17 to 0.30 wt%) resulted in an increase of the average crystal size from 92 to 151 μm after a 7-day heat treatment at 900 °C. Similar to the effect of increasing Cr_2O_3, increasing Fe_2O_3 concentrations (from 14.4 to 17.5 wt%) also increased the average crystal size.

These contrasting results indicate that melts in the previous study [17] contained nucleation agents that were absent in studies by Matyas et al. [20]. One obvious difference is a larger content of Cr in melts, which were formulated with an increased Cr content intended to protect melter walls against refractory corrosion. Chromium oxide has low solubility in the melt [21], which often results in an increased T_L and initiation of spinel formation before other components (Ni, Fe, Mn).

To determine the impact of glass composition on spinel crystal size, the Ni1.5 glass that precipitates large spinel crystals was mixed at various ratios with glasses such as CT16-IL-03 or CT16-OL-02 [17] that precipitate ~5 μm sized spinel crystals. The crystal size in the resulting glass was measured as a function of Ni1.5 content (from 0 to 100%) in the mixture. The CT16-IL-03 glass, *i.e.* IL-03, was chosen as it was the centroid composition of the statistically-designed matrix in a previous study [17]. The CT16-OL-02 glass from the same study, *i.e.* OL-02, was selected because it does not contain RuO_2, a known nucleation agent [15]. Hence, the aim of mixing IL-03 and OL-02 with Ni1.5 was to understand the impact of composition on crystal size, including the effects of RuO_2.

The spinel content was determined with X-ray diffraction (XRD) and the spinel crystal sizes determined by scanning electron microscopy (SEM). The T_L was measured for the primary, or parent, glasses, and estimated for all other glasses. In the glass melter and laboratory experiments the time available for crystal growth may not allow phase equilibrium to be reached and the final size of crystals can be affected by the crystal growth rate, which is controlled by diffusion. According to the Stokes-Einstein equation, the rate of diffusion is indirectly proportional to viscosity. The melt viscosity was estimated for all glasses, and measured for a subset of glasses, to check whether the final crystal size was achieved during isothermal heat treatments of set duration.

Table 1
Compositions of parent glasses in wt%.

Components	Ni1.5	IL-03	OL-02
Al_2O_3	8.14	13.00	10.61
B_2O_3	7.92	14.00	6.00
Cr_2O_3	0.17	1.00	0.33
Fe_2O_3	14.38	10.00	18.55
Li_2O	1.97	1.65	3.87
MnO	0.35	2.00	6.12
Na_2O	18.50	15.00	8.50
NiO	1.50	1.10	0.09
SiO_2	39.96	34.15	37.77
CaO	0.57	1.30	1.30
F	0.01	0.20	0.20
K_2O	0.34	0.45	0.45
La_2O_3	0.22	0.50	0.50
MgO	0.13	0.30	0.30
P_2O_5	0.32	1.30	1.30
ZrO_2	4.12	2.25	2.37
SO_3	0.08	0.00	0.00
TiO_2	0.03	0.00	0.00
ZnO	0.02	0.00	0.00
Cl	0.02	0.00	0.00
Ce_2O_3	0.20	0.00	0.00
CoO	0.01	0.00	0.00
CuO	0.04	0.00	0.00
Nd_2O_3	0.18	0.00	0.00
SnO_2	0.10	0.00	0.00
BaO	0.09	0.00	0.00
CdO	0.64	0.00	0.00
RuO_2	0.00	0.05	0.00
Ag_2O	0.00	0.05	0.05
Bi_2O_3	0.00	1.20	1.20
PbO	0.00	0.50	0.50

2. Experimental

2.1. Glass preparation

The parent glasses (Table 1) were prepared in 500 g portions from oxides and carbonates of 99% purity or greater and RuO_2 was added as ruthenium (III) nitrosylnitrate solution. The batches were mixed in an agate milling chamber of an Angstrom vibratory mill and melted at 1150 to 1200 °C in covered Pt-10% Rh crucibles (~1000 mL) for 1 h. The melt was poured onto a stainless-steel quench plate, allowed to cool to room temperature, ground, and mixed in a tungsten carbide milling chamber in the same vibratory mill for 4 min and remelted for 1 h at 1150 °C. Glasses that appeared inhomogeneous after the second melt, primarily mixed glasses with 50% or more of IL-03 and OL-02, were melted again under the same conditions as the first melt.

Two series of glasses for the spinel crystallization study were prepared by mixing 0–100 wt% Ni1.5, in 25 wt% increments, with either IL-03 or OL-02 glass. Prior to mixing, the individual glasses were crushed to a fine powder in the tungsten carbide milling chamber for 3 min. After crushing, the powders (150 g total) were mixed in varying amounts and homogenized in the agate mill chamber for 4 min. The mixed powders were subsequently melted in covered Pt-10% Rh crucibles at 1150 °C for 1 h. Melts were poured into 1 cm^3 platinum boats and cooled to room temperature before heat treatment.

2.2. Crystal characterization

The glass-filled platinum boats were placed in a furnace preheated at 1150 °C and held for 1 h, then the temperature was decreased to 900 °C and kept for 24 h. After 24 h, the samples were transferred to an annealing furnace for 1 h at 450 °C prior to allowing the furnace to cool to room temperature. The cooled samples were cut diagonally for analysis via XRD and SEM. Heat treat-

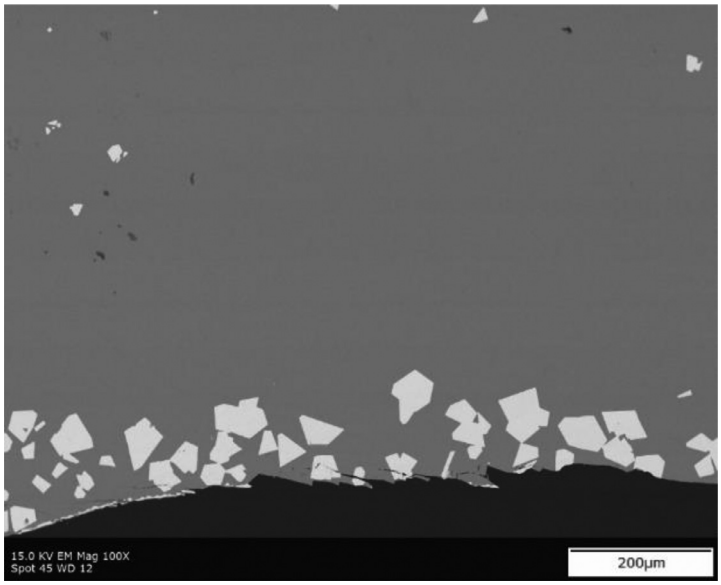

Fig. 1. BSE micrograph of Ni1.5 sample heat treated at 900 °C for 24 h showing spinel crystals (white), glass matrix (gray), and epoxy (black).

ments and sample preparation were completed according to ASTM C1720, Section 12.3.2 [22].

For quantitative XRD, samples were mixed with 5 wt% CaF_2 (internal standard) in a tungsten carbide milling chamber accessory in the vibratory mill for 2 min. The XRD pattern was collected using a Bruker D8 Advance X-ray diffractometer (Bruker AXS Inc., Madison, WI, USA) equipped with a Cu Kα target (λ = 1.5406 Å) at a power level of 40 kV and 40 mA, goniometer radius of 250 mm, fixed divergence slit 0.3°, and a LynxEye^{TM} position-sensitive detector. The scan settings range (2θ) was 5°–71°, step size 0.015°, and the minimum hold time 1.5 s/step. Bruker AXS© EVA (version 4) and Bruker Topas (version 4.2) software programs were employed to identify and quantify phase assemblages, respectively. For phase identification, Rietveld refinements were performed using whole pattern fitting according to the fundamental parameters approach and the Inorganic Crystal Structure Database version 2014-2. The main file used for fitting the XRD data was ICSD #94872 for trevorite. An example diffractogram is shown in supplemental information.

For microscopic analysis, samples were mounted in quick-setting epoxy (Allied High Tech Products, Inc.) and allowed to set for at least 1 h. The glasses were then polished on a Buehler EcoMet^{TM}/AutoMet 250 automatic polisher with silicon carbide polishing pads in the grit sequences 240, 320, 400, 600, 800, and 1200. The final steps were performed using felt polishing pads with 3 µm and 1 µm diamond particles in aqueous suspension. Crystalline phases were identified using a JEOL JSM-7001F field emission SEM instrument for collection of all backscattered electron (BSE) micrographs. BSE imaging was used to achieve atomic number contrast. Images were taken with a chamber pressure of 30 Pa (low-vacuum mode), 15 kV acceleration voltage, objective lens aperture 4, and a working distance of 10 mm. No conductive coating was applied. Image analysis was done with Adobe Photoshop CS6.

Magnification calibration was accomplished by imaging a National Institute of Standards and Technology (NIST)-certified magnification standard (NIST SRM 8820) under imaging conditions identical to those used for each specimen. To verify the scales used for analysis, the length of a known feature size on the standard was measured in pixels on the digital image to obtain the number of pixels per unit length. After length calibration, the crystal size was determined by selecting all the spinel crystals in the image by capitalizing on the high contrast between the dark gray glass matrix and the white spinel crystals.

The average crystal size was measured in Photoshop, by "Record Measurements" and the Ruler Tool. For each sample, 70 or more crystals, or features, were used to arrive at the average crystal size reported in this text. The average linear size of the triangular and rectangular sections of the octahedrons that made occasional twins and agglomerates does not represent the true length of crystals captured [23,24], but the results are assumed to be reasonably representative for the purpose of relative comparison.

2.3. Liquidus temperature and viscosity

T_L was determined following the ASTM-C1720-11 standard [22]. Samples were heat treated in 1 cm^3 platinum boats for 72 h at temperatures below 900 °C, for 24 h at temperatures between 900 °C and 1250 °C, and for 6 h at temperatures above 1250 °C. T_L was determined by extrapolating the crystal fraction versus temperature to zero [25].

Glass melt viscosity was measured with a rotational Anton Paar viscometer (model FRS1600) in a Pt-10%Rh crucible with a Pt-10%Rh cylindrical spindle in samples equilibrated for 60 min at 1150 °C, 1050 °C, 950 °C, 1150 °C, 1250 °C, and 1150 °C in the order of measurement sequence. The shear stress was measured over a 3 min period at a shear rate of 10 s^{-1}.

3. Results

3.1. Crystal mass fraction and crystal size

Spinel precipitated from the parent glasses (Ni1.5 [20], IL-03 [17], and OL-02 [17]) as the only crystalline phase present. Figs. 1, 2, and 3 show SEM images of spinel crystals in glass samples heat treated for 24 h at 900 °C.

Tables 2 and 3 list spinel mass fractions and the average spinel sizes, respectively, in the Ni1.5–IL-03 and Ni1.5–OL-02 glass mixtures. As expected, more spinel precipitated at 900 °C than at 1150 °C and in Ni1.5–OL-02 glasses than in Ni1.5–IL-03 glasses,

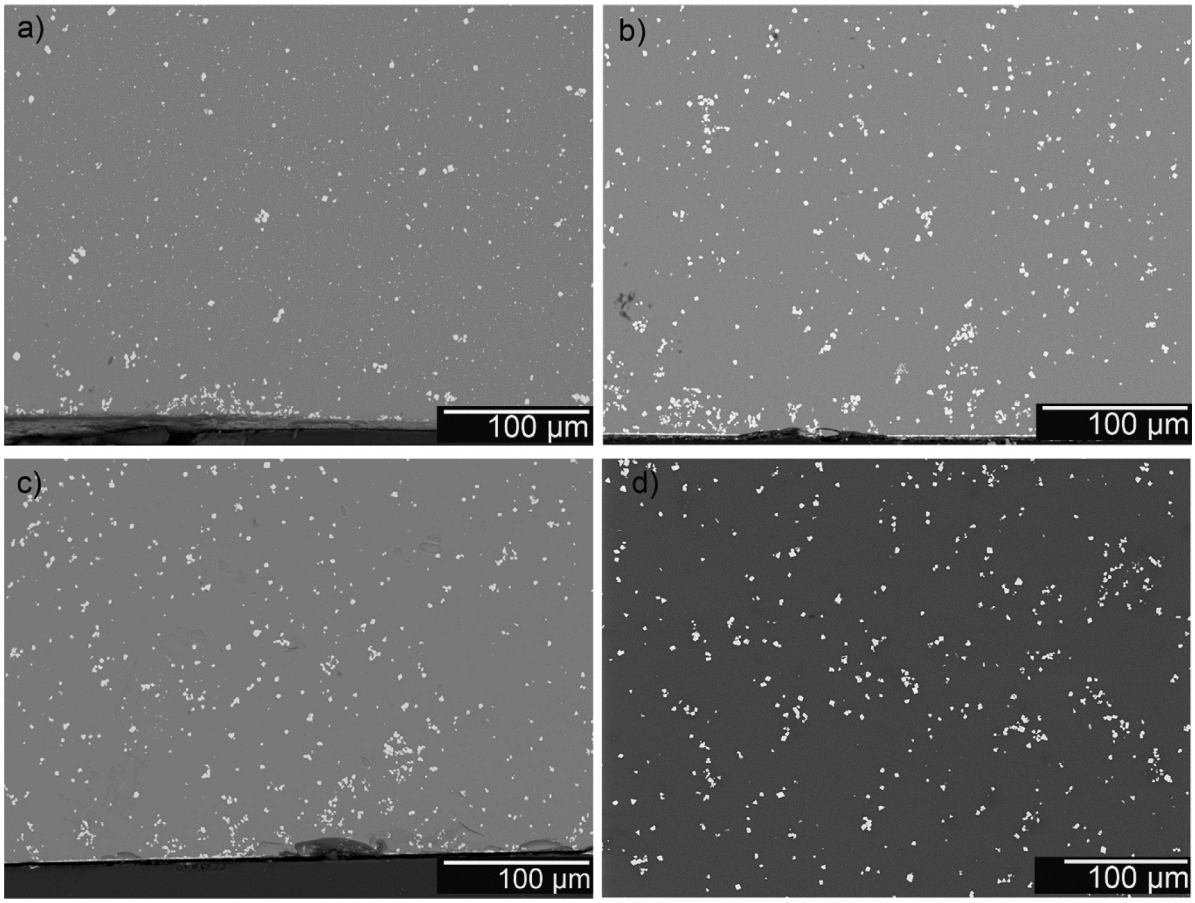

Fig. 2. BSE micrographs of Ni1.5–IL-03 samples with 75 (a), 50 (b),25 (c), and 0 (d) wt% of Ni1.5. Glasses were held at 900 °C for 24 h. Spinel crystals are white and the glass matrix is gray.

Table 2
Spinel mass fraction in samples quench from 1150 °C and heat treated for 24 h at 900 °C.

Ni1.5 Glass(wt%)	Spinel Fraction (wt%)			
	Ni1.5–IL-03		Ni1.5–OL-02	
	Quenched from 1150 °C	Heat Treated at 900 °C for 24 h	Quenched from 1150 °C	Heat Treated at 900 °C for 24 h
0	3.4	5.1	7.1	12.9
25	2.2	4.1	3.4	10.4
50	1.4	3.4	1.2	5.4
75	0	3.4	0	3.3
100	0	4.4	0	4.4

Table 3
Average size of spinel crystals in samples heat treated for 24 h at 900 °C.

Ni1.5 Glass (wt%)	Average Crystal Size (µm)	
	IL-03	OL-02
0	3.8	5.7
25	3.1	9.6
50	2.7	10.4
75	1.2	18.3
100	42.3	

which contained less spinel-forming components such as Fe_2O_3 and MnO (Table 1).

For melts heat treated for 24 h at 900 °C, the average crystal size was 3.8 μm in IL-03 glass, 5.7 μm in Ru-free OL-02 glass, and 42.3 μm in Ni1.5 glass. The largest crystals in Ni1.5 were 77 μm, similar to previously reported values [5,20]. Crystal sizes were near or below 5 μm in the Ni1.5+IL-03 series (Fig. 2). In the Ni1.5–OL-02 series (Fig. 3), crystal sizes varied from 5.7 μm at 0 wt% Ni1.5 to ~10 μm at 25 and 50 wt% Ni1.5, 18.3 μm at 75 wt% Ni1.5, 42.3 μm at 100 wt% Ni1.5 (Fig. 1).

3.2. Liquidus temperature

Fig. 4 displays the spinel fraction (listed in Tables 2 and 3) versus temperature for Ni1.5 (a) and IL-03 (b). The spike at 1300 °C in Fig. 4b (the red dot) was caused by crystallization during quenching, *i.e.* formation of secondary crystals, as previously observed by Riley et al. [16]. The secondary crystals are on the order of hundreds of nanometers, as shown in Fig. 5. The crystals that were < 1 μm formed outside the diffusion "aura", defined as a re-

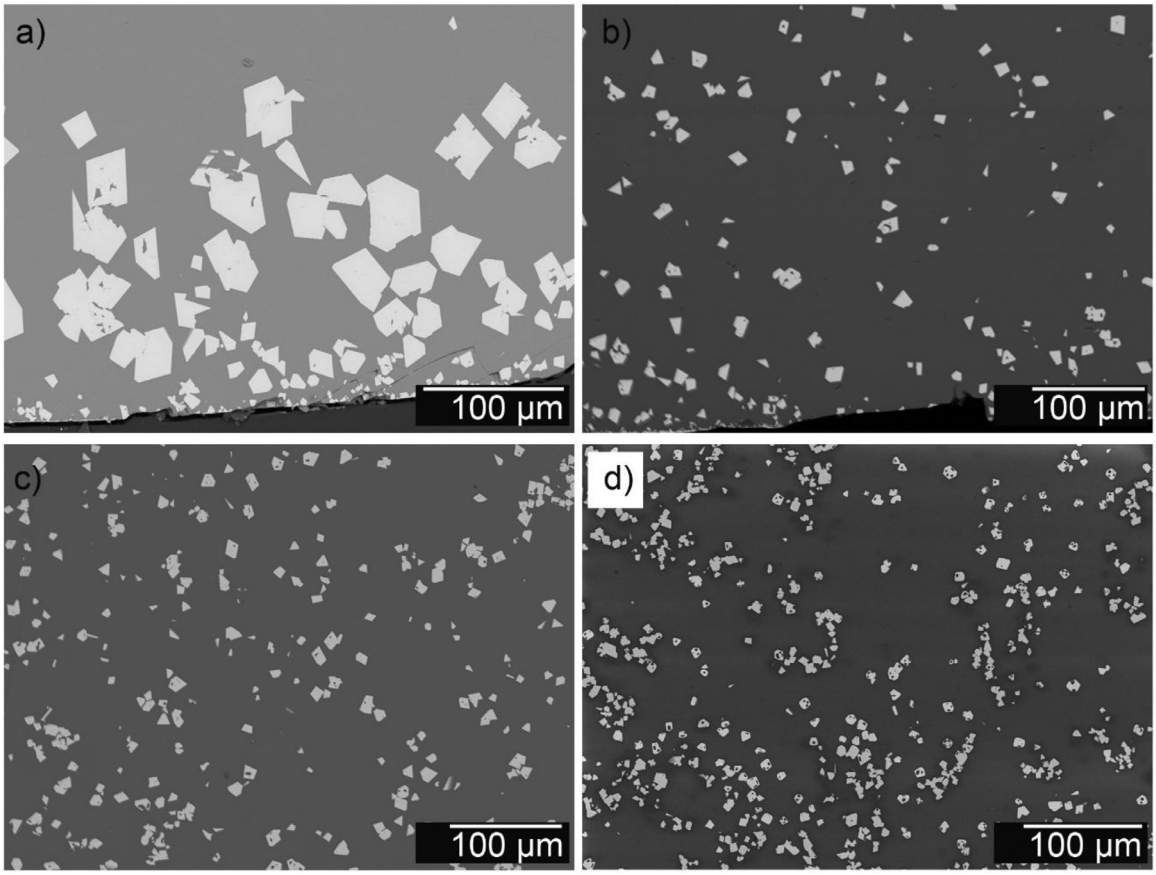

Fig. 3. BSE micrographs of Ni1.5–OL-02 samples with 75 (a), 50 (b),25 (c), and 0 (d) wt% of Ni1.5. Glasses were held at 900 °C for 24 h. Spinel crystals are white and the glass matrix is gray.

Table 4
Liquidus temperature component coefficients [25].

Components	$T_{L,i}$ (°C)	Components	$T_{L,i}$ (°C)
Al_2O_3	3307	Na_2O	-1826
B_2O_3	395	NiO	8210
Cr_2O_3	18864	SiO_2	834
Fe_2O_3	2644	MgO	2827
Li_2O	-1470	Others	4419
MnO	1870	–	–

Table 5
Measured and estimated liquidus temperatures for the Ni1.5–IL-03 and Ni1.5–OL-02 mixtures; NM = not measured.

Amount of Ni1.5 Glass(wt%)	IL-03 Measured (°C)	Estimated (°C)	OL-02 Estimated (°C)
100	1125	1122	1122
75	NM	1193	1218
50	NM	1264	1315
25	NM	1335	1411
0	1362	1406	1508

gion with decreased concentration of spinel-forming components, around the larger crystals during sample cooling.

T_L was determined by extrapolating the spinel fraction, prior to secondary crystal formation, to zero, resulting in T_L equal to 1125 °C for Ni1.5 and 1362 °C for IL-03. For all other glasses, the T_L was estimated using a first-order model:

$$T_L = sum(T_{L,i}x_i) \quad (2)$$

where $T_{L,i}$ is the ith liquidus temperature component coefficient and x_i is the ith component mass fraction in glass. The model coefficients are reported in [25] and listed in Table 4. The "Others" component accounts for components not shown in the table, *e.g.* RuO_2. Table 5 shows estimated and measured T_L values.

For Ni1.5 and IL-03 glasses, the estimated T_L values are off by 44°C (3% relative to measured) for IL-03 glass and by 3°C (0.2% relative to measured) for Ni1.5 glass, giving confidence in estimated values. The estimated T_L values of IL-03 series are lower than those of OL-02 series, as IL-03 possesses higher fractions of Cr_2O_3 and NiO as well as higher Na_2O and B_2O_3. In contrast, OL-02 has significantly less Na_2O and more Fe_2O_3 and MnO (Table 1), all of which have been shown to strongly affect T_L (Table 4).

3.3. Melt viscosity

Fig. 6 displays measured viscosity data for Ni1.5 and IL-03 glasses as a function of inverse temperature. The linear trendlines show that:

$$ln(\eta) = A + \frac{B}{T} \quad (3)$$

where the intercept, A, and the slope, B, are listed in the legends. For HLW glasses, A is independent of glass composition and B is a linear function of component mass fractions [26]. Because the ith component mass fraction of the Ni1.5–IL-03 mixed glasses is:

$$x_i = zx_{Ni1.5} + (1-z)x_{IL-03} \quad (4)$$

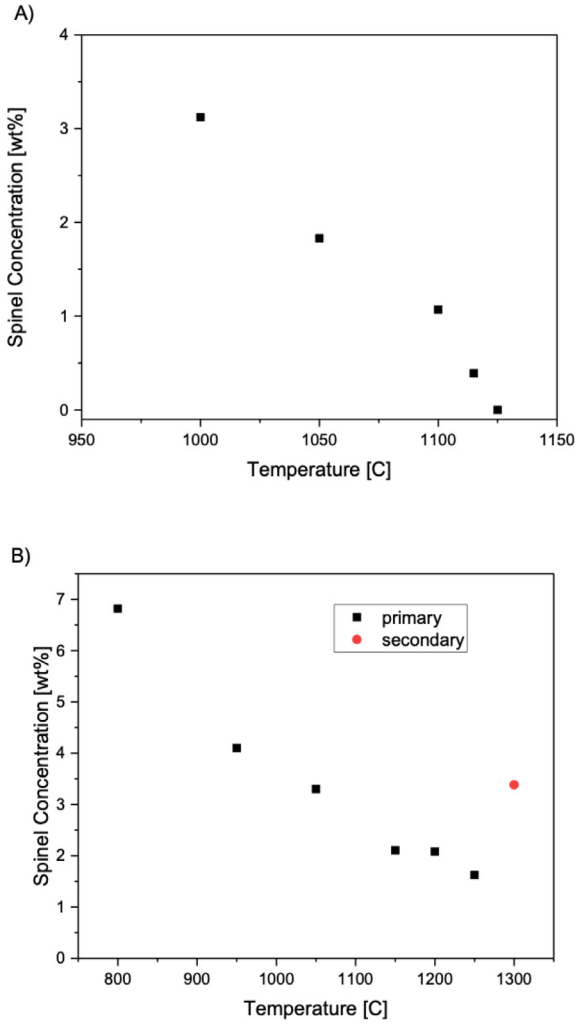

Fig. 4. Spinel concentration versus temperature for a) Ni1.5 and b) IL-03.

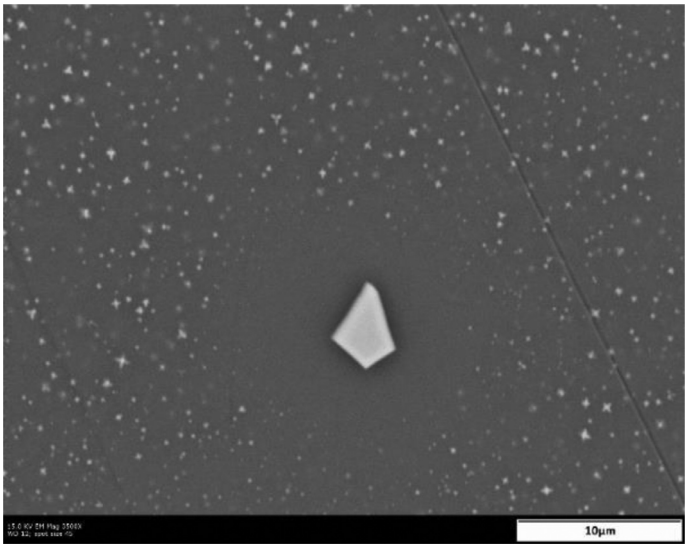

Fig. 5. Secondary spinel crystals formed in the IL-03 sample after heat treatment at 1300 °C for 6 h.

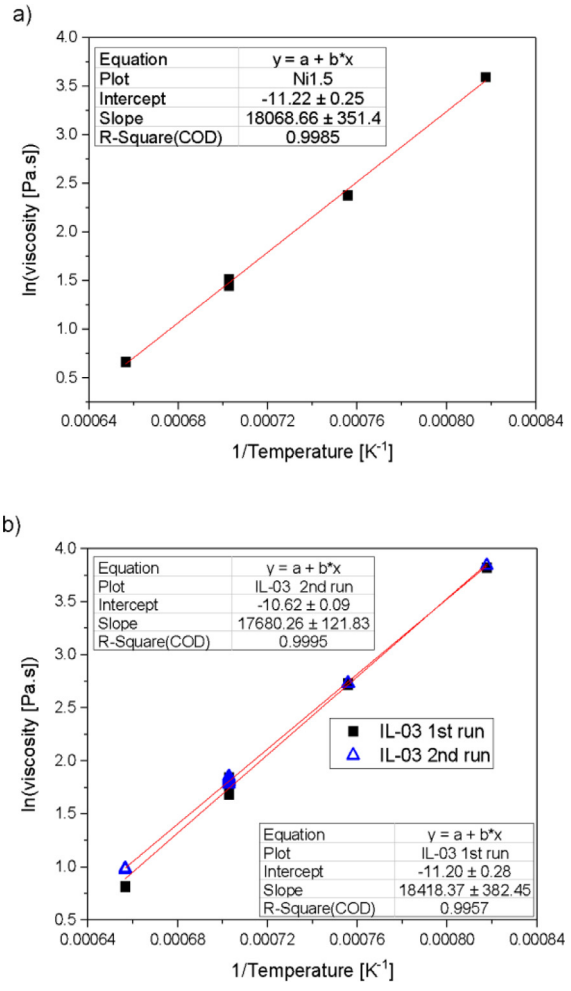

Fig. 6. Viscosity versus temperature for (a) Ni1.5 and b) IL-03 glasses.

Table 6
Measured (*) and estimated viscosities of Ni1.5–IL-03 and Ni1.5–OL-02 mixtures at 900 °C.

Ni1.5 Glass(wt%)	Viscosity at 900°C (Pa•s)	
	IL-03	OL-02
0	88.0*	76.5
25	81.8	73.6
50	76.0	70.9
75	70.6	68.2
100	65.6*	65.6

where z is the Ni1.5 glass fraction in the mixture, it is reasonable to assume that the viscosity of a mixed glass is given by the formula:

$$ln(\eta) = zln(\eta_{Ni1.5}) + (1-z)ln(\eta_{IL-03}) \quad (5)$$

Table 6 lists measured and estimated viscosities at 900 °C. The value of η_{IL-03} is an average of the two runs shown in Fig. 6b. The second run was performed after holding at 900 °C. As Fig. 7 shows, during the viscosity measurement, crystals grew near the top portion of the molten sample, likely causing a slightly higher viscosity measurement for the second IL-03 run. Viscosity of the OL-02 glass was not measured and was estimated using component coefficients from the literature [26].

Fig. 7. Photograph of IL-03 glass after the viscosity measurement: (a) top portion of the quenched glass; (b) the bulk glass (≥ 80% of volume) after measurement.

4. Discussion

4.1. Effect of mixing ratio on crystal size

This study used a two-glass mixture approach, with each individual glass being a multicomponent mixture. As a rule, the ratio at which two glasses are blended would generally preclude attributing the observed changes in properties to any single component of the mixture because the fractions of individual components in the original glasses are correlated. Quantification of individual component effects on spinel crystal size was not the initial purpose of this study; the goal was to find out whether the crystal size would change gradually or abruptly with the ratio of mixing.

Table 3, Figs. 1, 2, and 8, show a 35-fold decrease in crystal size when 25 wt% of the RuO_2-containing IL-03 glass (the minimum fraction tested) was mixed with the Ni1.5 glass. Mixing increasingly larger fractions of the IL-03 glass with the Ni1.5 glass made minor changes (from 1.2 to 2.8 μm), which are within the impacts of expected variations in experimental parameters such as temperature of furnace, time for heat treatments, etc. that may influence crystal size. The mixture of 25 wt% IL-03 glass with 75 wt% Ni1.5 glass contains 0.01 wt% RuO_2 (see Table 1), which was enough to nucleate a large number of small spinel crystals (Fig. 2a).

Table 3, Figs. 1, 3, and 8, show the response of the crystal size to the Ni1.5–OL-02 mixing ratio that did not contain RuO_2. The change in crystal size with the mixing ratio was more gradual, relative to the Ni1.5–IL-03 series. However, the 25 wt% addition of OL-02 glass mixed with the Ni1.5 glass still results in an over 2-fold decrease in average crystal size from 42 to 18 μm.

Mixing a glass producing small crystals of spinel (~5 μm) with a glass producing large spinel crystals (~50 μm) leads to a sharp decrease in the crystal size in the mixed glass even when

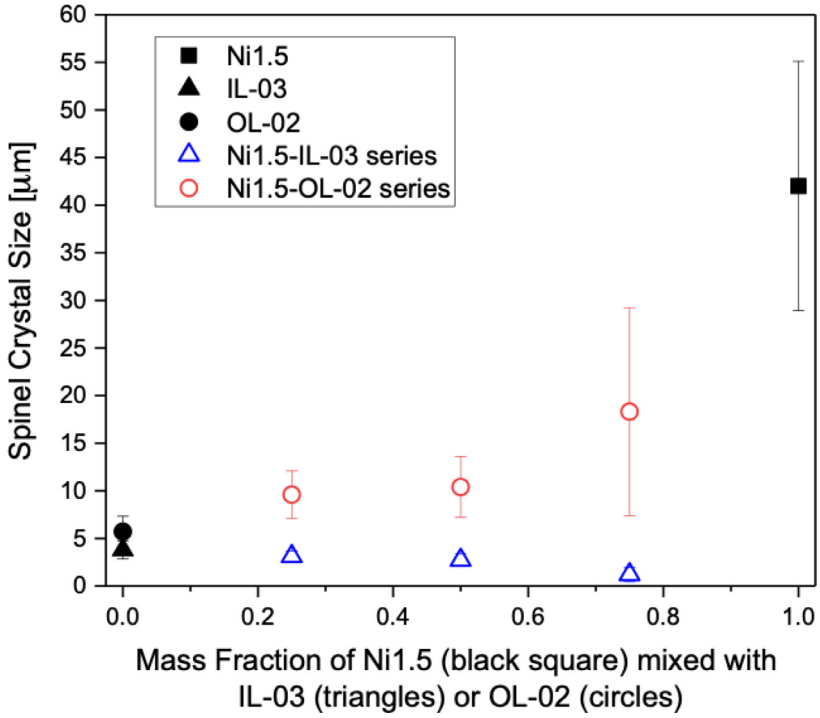

Fig. 8. Average crystal sizes after heat treatment at 900 °C for 24 h versus mass fraction of Ni1.5 (black square) in the Ni1.5–IL-03 glasses (blue triangles) and in Ni1.5–OL-02 series glasses (red circles). The black symbols indicate the three parent glasses.

the added fraction is relatively small (25 wt%). If the added glass has a powerful nucleation agent (RuO_2) the minimum crystal size (~5 μm) is reached with relatively small additions (25 wt%). In the absence of such an agent, further additions lead to a gradual change of crystal size.

4.2. Effect of nucleation rate

Fig. 9 shows crystal size as a function of T_L and Cr_2O_3 content. Fig. 9a plots the crystal size of glasses heat treated at 900 °C versus T_L values listed in Table 5. In the Ni1.5–IL-03 series, the difference between T_L and the heat-treatment temperature did not influence the crystal size that has already been determined by the nucleation sites from RuO_2. This can be seen by minimal changes in crystal size when T_L becomes greater than 1175 °C. For the Ni1.5–OL-02 series, which did not contain RuO_2, the effect of the T_L on crystal size was notably different.

A higher T_L causes a higher rate of nucleation during the constant-temperature heat treatment (900 °C), resulting in a higher crystal number density and a smaller crystal size [19]. As the liquidus temperature coefficient of Cr_2O_3 being exceptionally high, 18864 °C (Table 4), it influences the T_L more strongly than any other glass component. Therefore, it appears that Cr_2O_3 significantly contributes to the large number of seeds in the mixed glasses. Fig. 9b shows a plot of crystal size versus Cr_2O_3 concentration. There is little impact of Cr_2O_3 on Ni1.5–IL-03 series, where the presence of RuO_2 was dominant, but the effect on the Ni1.5–OL-02 series is prominent.

Hence, the large number of seeds in blended glasses coming from the premelted OL-02 and IL-03 glasses naturally resulted in smaller crystals even when the fraction of OL-02 and IL-03 glasses in the mixture was relatively small (25 wt%).

4.3. Effect of viscosity

The high crystal number density seen in Figs. 2d and 3d indicates that the melts reached phase equilibrium during the heat treatment at 900 °C. The distances between crystals were relatively short, and thus 24 h allows sufficient time for diffusion of the spinel-forming species to the crystals from the surrounding melt. Accordingly, the average crystal sizes of ~5 μm are the equilibrium sizes for the associated compositional region. The time needed for a diffusion process to reach equilibrium is proportional to the square of the diffusion distance, which decreases with decreasing crystal number density, so the potential effect of crystal growth rate on the crystal size can be considered for the Ni1.5 glass and even some glasses of the Ni1.5–OL-02 series that produced crystals of ~10 μm or larger. If this effect exists, *i.e.* the final crystal size after the heat treatment is affected by diffusion, it would be more pronounced for compositions with a low diffusion coefficient or with a high viscosity.

Fig. 10 plots the crystal size after heat treatment at 900 °C for 24 h against melt viscosity, which is inversely proportional to the diffusion coefficient. The trends are similar to those displayed in Fig. 8, in which they are explained as result of the crystal number density. Consequently, if large crystals formed in melts of high viscosity have not reached their maximum sizes, such an effect cannot be discerned from the current data. The effect of the crystal number density is dominant and the crystal size is controlled by the rate of nucleation, rather than by crystal growth rate, which is governed by diffusion. This conclusion can be further supported using the Stokes-Einstein equation:

$$D = \frac{k_B T}{6\pi r \eta} \tag{6}$$

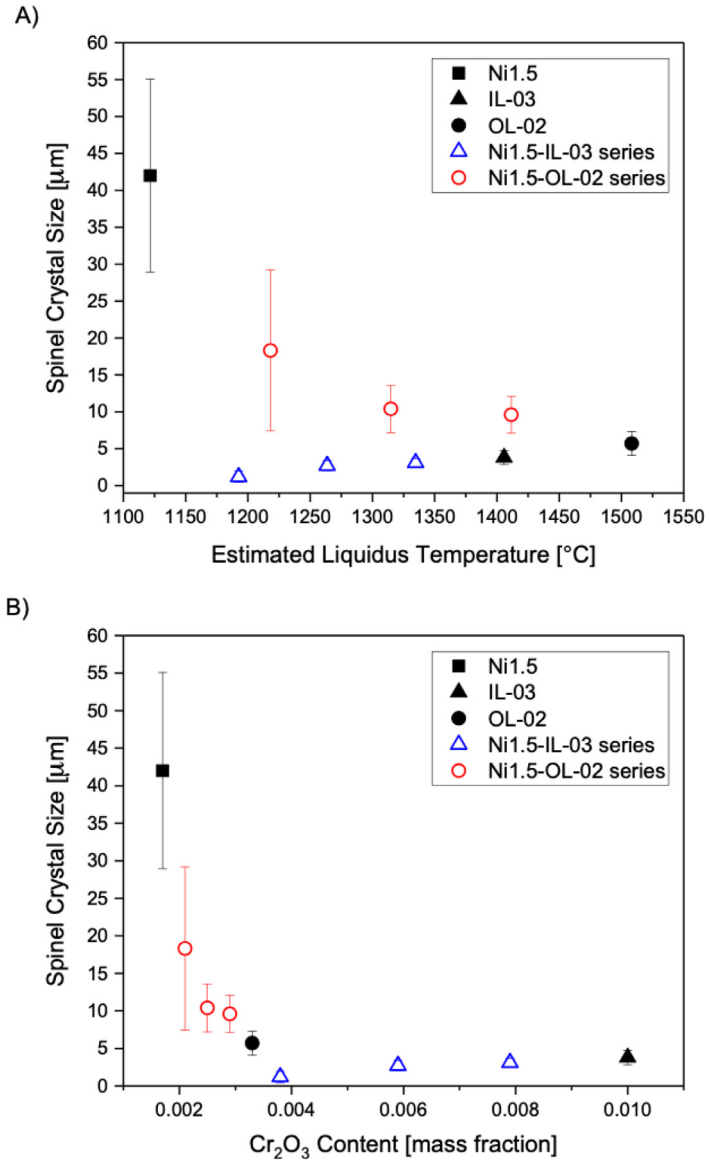

Fig. 9. Average crystal sizes after heat treatment at 900 °C for 24 h for Ni1.5+IL-03 glasses (blue triangles) and in Ni1.5+OL-02 glasses (red circles) versus liquidus temperature (a) and Cr_2O_3, in mass fraction (b); black solid symbols indicate the parent glasses.

where k_B is the Boltzmann constant (1.38×10^{-23} $m^2kg\ s^{-2}K^{-1}$) and r is the oxygen atomic radius (m). For molten glass at $T = 1400$ K and $\eta = 2$ Pa s, $D = 5 \times 10^{-13}$ m^2s^{-1}. The characteristic diffusion distance to reach equilibrium is then:

$$x = \sqrt{Dt} \tag{7}$$

After a 24 h heat treatment, we can estimate that x ≈ 200 μm. As Fig. 3 shows, the distance between crystals is significantly shorter than 2x. Thus, one can safely conclude that phase equilibrium was reached during all heat treatments.

4.4. Potential impact on Hanford mission

The results presented indicate that glass melts lacking noble metals as nucleation agents can still precipitate spinel crystals small enough to prevent their settling in the melter or in the discharge riser if the content of chromium oxide in these melts is high enough. Spiking waste glasses with chromium oxide has already been considered to protect the melter walls against corrosion [27], so chromium oxide addition may now serve a double purpose. The inclusion of chromium oxide to glass melts may extend the melter lifetime and shorten the Hanford cleanup mission via formulating glasses with an increased waste loading when the spinel constraint is relaxed.

A question arises as to whether the outcome seen in this work can be reproduced if melter feeds are batched instead of mixing premelted glasses and if the crystals are produced in the cold cap from the slurry feed charged into the joule-heated melter. More data are needed regarding the formulation of melter feeds to limit spinel size in the melter during idling or in the melter discharge riser. Regardless, the current study shows that the size of spinel crystals can be controlled by varying glass chemistry, in particular, the presence, or absence, of RuO_2 and the fraction of Cr_2O_3 in the melt.

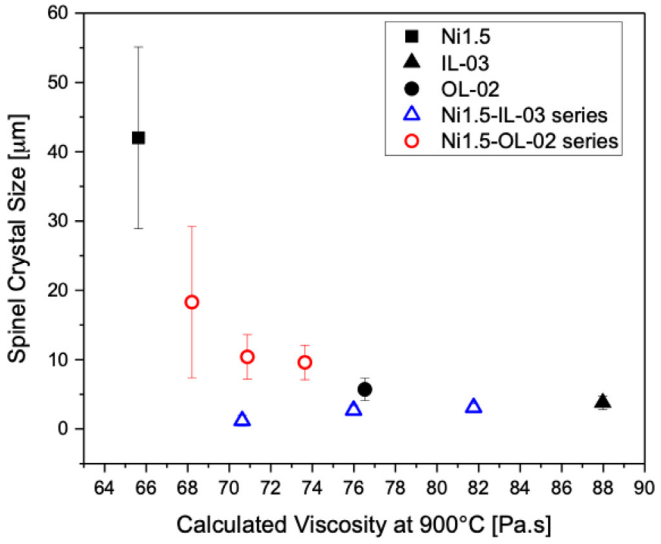

Fig. 10. Average crystal sizes after heat treatment at 900 °C for 24 h versus melt viscosity at 900 °C.

5. Conclusions

Mixing a glass with an average spinel crystal size of around 5 μm with a glass that grew spinel crystals of an average size of approximately 42 μm (max crystal size = 77 μm) revealed that RuO_2 and Cr_2O_3 were the most impactful components on the resulting crystal size. The presence of RuO_2, a known nucleating agent, in one mixture (Ni1.5–IL-03) resulted in a small size of spinel crystals. Increased Cr_2O_3 concentration resulted in the formation of small spinel crystals in the mixed glasses without RuO_2. It is clear that the presence of RuO_2 (a common HLW component) and Cr_2O_3 (a component that can aid in reducing refractory corrosion) at relatively higher concentrations can lend to the formation of smaller crystals which can increase the tolerance for spinel in waste glass melters, allowing for a substantial increase in waste loading.

Author credits

Charmayne Lonergan managed the experimental work, contributed heavily to the writing of the manuscript, as well as performed a significant portion of data analysis.

Jarrett Rice performed the experimental work and some data analysis.

Chloe Skidmore performed the experimental work and provided editing support.

Michael Schweiger managed some of the experimental work, contributed to writing and editing, and contributed to data analysis.

Pavel Hrma contributed significantly to data analysis and manuscript writing.

Declaration of Competing Interest

The authors declare that they have no known competing financial interests or personal relationships that could have appeared to influence the work reported in this paper.

CRediT authorship contribution statement

C.E. Lonergan: Visualization, Writing – original draft, Formal analysis. **J. Rice:** Visualization, Formal analysis. **C. Skidmore:** Visualization, Writing – original draft. **M.J. Schweiger:** Visualization, Writing – review & editing, Formal analysis. **P. Hrma:** Writing – original draft, Formal analysis.

Acknowledgements

The authors would like to thank John Vienna, Renee Russell, Jaime George, Tongan Jin, James Neeway, Brian Riley, and Seung Min Lee for their reviews as well as Matt Wilburn for technical editing support. Additionally, the authors gratefully acknowledge the financial support provided by the U.S. Department of Energy Office of River Protection's Waste Treatment and Immobilization Plant project, managed by Tom Fletcher, with technical oversight by Dr. Albert Kruger. Manuscript completion was also funded, in part, by a PNNL Laboratory Directed Research and Development effort.

Supplementary materials

Supplementary material associated with this article can be found, in the online version, at doi:10.1016/j.jnucmat.2021.153318.

References

[1] R.A. Peterson, E.C. Buck, J. Chun, R.C. Daniel, D.L. Herting, E.S. Ilton, G.J. Lumetta, S.B. Clark, Review of the scientific understanding of radioactive waste at the U.S. DOE Hanford site, Environ. Sci. Technol. 52 (2018) 381–396.
[2] J.D. Vienna, Compositional models of glass/melt properties and their use for glass formulation, Proc. Mater. Sci. 7 (2014) 148–155.
[3] J.D. Vienna, G.F. Piepel, D.S. Kim, J.V. Crum, C.E. Lonergan, B.A. Stanfill, B.J. Riley, S.K. Cooley, T. Jin, 2016 Update of hanford glass property models and constraints for use in estimating the glass mass to be produced at Hanford by implementing current enhanced glass formulation efforts, PNNL-25835 Rev. 0, Pacific Northwest National Laboratory, Richland, WA (2016) doi:10.2172/1772236.
[4] A.A. Kruger, C.P. Rodriguez, J.B. Lang, A.R. Huckleberry, J. Matyas, A.T. Owen, Crystal-tolerant glass approach for mitigation of crystal accumulation in continuous melters processing radioactive waste, ORP-52717, Rev. 0, U.S. Department of Energy, Office of River Protection, Richland, WA (2012).
[5] J. Matyas, J.D. Vienna, A. Kimura, M. Schaible, R.M. Tate, Development of crystal-tolerant waste glasses, Cer. Trans. 222 (2010) 41–51.
[6] G.F. Piepel, S.K. Cooley, A. Heredia-Langner, S.M. Landmesser, W.K. Kot, H. Gan, I.L. Pegg, IHLW PCT, Spinel $T_{1\%}$, Electrical Conductivity, and Viscosity Model Development, U.S. Department of Energy, Office of River Protection, Richland, WA, 2008 VSL-07R1240-4, ORP-56320, doi:10.2172/1105987.
[7] D.S. Kim, J.D. Vienna, G.L. Smith, S.K. Sundaram, D.R. Spearing, Influence of glass property restrictions on Hanford HLW glass volume, in: Environmental Issues and Waste Management Technologies in the Ceramic and Nuclear Industries VII, 132, American Ceramic Society, 2002, pp. 105–115.
[8] J.H. Christian, Crystallization in High-Level Waste Glass: A Review of Glass Theory and Noteworthy Literature, Savannah River National Laboratory, Aiken, SC, 2015 SRNL-STI-2015-00415, Rev. 0.
[9] V. Jain, S.M. Barnes, T.K. Vethanayagam, L.D. Pye, Noble metal and spinel deposition on the floor of the joule-heated ceramic melter, J. Am. Cer. Soc. 74 (1991) 1559–1562.
[10] J. Matyas, A.R. Huckleberry, C.P. Rodriguez, J.B. Lang, A.T. Owen, A.A. Kruger, HLW Glass Studies: Development of Crystal-Tolerant HLW Glasses, Pacific Northwest National Laboratory, Richland, WA, 2012 PNNL-21308.
[11] W.N. Rankin, P.E. O'Rourke, P.D. Soper, M.B. Cosper, B.C. Osgood, Evaluation of Corrosion and Deposition in the 1941 Melter, Savannah River Laboratory, Aiken, SC, 1982 DPST-82-231.
[12] J.D. Vienna, D.S. Kim, Preliminary IHLW Formulation Algorithm Description, 24590-HLW-RPT-RT-05-001, Rev. 0, River Protection Project, Hanford Waste Treatment and Immobilization Plant, Richland, WA, 2008.
[13] J.D. Vienna, D.S. Kim, D.C. Skorski, J. Matyas, Glass Property Models and Constraints for Estimating the Glass to be Produced at Hanford by Implementing Current Advanced Glass Formulation Efforts, Pacific Northwest National Laboratory, Richland, WA, 2013 PNNL-22631, Rev. 1 (ORP-58289).
[14] P. Hrma, Crystallization during processing of nuclear waste glass, J. Non Cryst. Solids 356 (2010) 3019–3025.
[15] J. Alton, T.J. Plaisted, P. Hrma, Nucleation and growth of spinel crystals in a borosilicate glass, J. Non Cryst. Solids 311 (2002) 24–35.
[16] B.J. Riley, P. Hrma, J.V. Crum, J.D. Vienna, M.J. Schweiger, C.P. Rodriguez, R.A. Peterson, Liquidus temperature in the spinel primary phase field: a comparison between optical and crystal fraction methods, J. Non Cryst. Solids 483 (2018) 1–9.
[17] C.E. Lonergan, K. Akinloye-Brown, J. Rice, V. Gervasio, N. Canfield, M.J. Schweiger, J.D. Vienna, Micron-sized spinel crystals in high level waste glass compositions: determination of crystal size and crystal fraction, J. Nucl. Mater. 514 (2019) 12.

[18] P. Isak, P. Hrma, B.W. Arey, T.J. Plaisted, Effect of feed melting, temperature history, and minor component additions on spinel crystallization in high-level waste glass, J. Non Cryst. Solids 289 (2001) 17–29.
[19] B.K. Wilson, P. Hrma, J. Alton, T.J. Plaisted, J.D. Vienna, The effect of composition on spinel equilibrium and crystal size in high-level waste glass, J. Mater. Sci. 37 (2002) 5327–5331.
[20] J. Matyas, J.E. Amonette, R.K. Kukkadapu, D. Schreiber, A.A. Kruger, T. Ohji, J. Matyas, N.J. Manjooran, G. Pickrell, A. Jitianu, The effects of glass doping, temperature and time on the morphology, composition, and iron redox of spinel crystals, in: Advances in Materials Science for Environmental and Energy Technologies III, 250, John Wiley & Sons, Inc., 2014, pp. 147–156.
[21] P. Hrma, J.D. Vienna, B.K. Wilson, T.J. Plaisted, S.M. Heald, Chromium phase behavior in a multi-component borosilicate glass melt, J. Non Cryst. Solids 352 (2006) 2114–2122.
[22] ASTM C1720-17Standard Test Method for Determining Liquidus Temperature of Waste Glasses and Simulated Waste Glasses, ASTM International, West Conshohocken, PA, 2017.
[23] M. Mendelson, Average grain size in polycrystalline ceramics, J. Am. Ceram. Soc. 52 (1969) 443–446.
[24] A.R.C. Gerlt, A.K. Criner, L. Semiatin, E.J. Payton, On the grain size proportionality constants calculated in M.I. Mendelson's "average grain size in polycrystalline ceramics, J. Am. Ceram. Soc. 102 (2018) 37–41.
[25] P. Hrma, J.D. Vienna, M. Mika, J.V. Crum, G.F. Piepel, Liquidus temperature data for DWPF glass, Pacific Northwest National Laboratory, Richland, WA, 1998 PNNL-11790.
[26] P. Hrma, A.A. Kruger, High-temperature viscosity of many-component glass melts, J. Non Cryst. Solids 437 (2016) 17–25.
[27] I.S. Muller, K. Gilbo, M. Chaudhuri, I.L. Pegg, K-3 Refractory Corrosion and Sulfate Solubility Model Enhancement, Catholic University of America, Washington, D.C., 2018 VSL-18R4360-1.